Case 3.3: Taylor-Green Vortex Evolution

Laslo T. Diosady * Scott M. Murman †

NASA Ames Research Center, Moffett Field, CA, USA

Code Description

This work uses a higher-order discontinuous-Galerkin finite-element method to solve the compressible Navier-Stokes equations [1,2]. The unsteady Navier-Stokes equations are discretized using a non-linearly stable space-time entropy-variable formulation. The inviscid flux is computed using the approximate Riemann solver of Ismail and Roe [3]. The viscous fluxes are computed using an interior penalty (IP) method equivalent to the second form of Bassi and Rebay (BR2) [4]. Evaluation of the integrals appearing in the DG formulation are performed using a dealiased quadrature rule using $2N$ points in each direction where N is the solution order (in either space or time). The nonlinear problem arising at each time-slab is solved using a Jacobian-free Newton-Krylov method using a diagonalized-ADI preconditioner [5]. Results are presented using the space-time formulation with accuracy up to 16th order ($N = 16$) in both space and time.

The code is parallelized using the Message Passing Interface (MPI). The computations presented in this work are performed using the Sandy Bridge nodes of the NASA Pleiades supercomputer at NASA Ames Research Center. Each Sandy Bridge node consists of 2 eight-core Intel Xeon E5-2670 processors with a clock speed of 2.6Ghz and 2GB per core memory. On a Sandy Bridge node the Tau Benchmark [6] runs in a time of 7.6s.

Case Description

The Taylor-Green vortex flow is simulated using the compressible Navier-Stokes equations at $M_0 = 0.1$. The flow is solved on an isotropic domain which spans $[0, 2\pi L]$ in each coordinate direction. The initial conditions are given by:

$$u = V_0 \sin(x/L)\cos(y/L)\cos(z/L) \quad (1)$$

$$v = -V_0 \cos(x/L)\sin(y/L)\cos(z/L) \quad (2)$$

$$w = 0 \quad (3)$$

$$p = \rho_0 V_0^2 \left[\frac{1}{\gamma M_0^2} + \frac{1}{16}\left(\cos(2x) + \cos(2y)\right)\left(\cos(2z) + 2\right)\right] \quad (4)$$

where u,v and w are the components of the velocity in the x, y and z-directions, p is the pressure and ρ is the density. The flow is initialized to be isothermal ($\frac{p}{\rho} = \frac{p_0}{\rho_0} = RT_0$). The flow is computed at a Reynolds number of $Re = \frac{\rho_0 V_0 L}{\mu} = 1600$, where μ is the viscosity. The Prandtl number is $Pr = 0.71$, while the bulk viscosity is given by the Stokes hypothesis: $\lambda = -\frac{2}{3}\mu$. The unsteady simulation is performed for $20t_c$, where $t_c = \frac{L}{V_0}$ is the characteristic convective time. The time-step is set based on maintaining a CFL of order 1 based on the convective speed, and resolution length and time scales. Specifically, we set $\Delta t = CFL\frac{hN}{M_0 c}$, where $CFL = 1$ is the Courant-Friedrichs-Lewy number, $h = DOF^{1/3}$ is the resolution length-scale, N is the solution order in the temporal direction, $M_0 = 0.1$ is the Mach number and c is the speed of sound.

*laslo.diosady@nasa.gov
†scott.m.murman@nasa.gov

Meshes

The Taylor-Green vortex was simulated using the space-time DG formulation using 2nd-,4th-,8th- and 16th-order in space and 4th-order in time. Direct numerical simulation was performed using six different mesh sizes for each polynomial order considered, such that the total number of degrees of freedom in each coordinate direction was 48, 64, 96, 128, 192, 256.

Results

For each run the temporal evolution of the kinetic energy

$$E_k = \frac{1}{\Omega}\int_\Omega \tfrac{1}{2}\rho \mathbf{v}\cdot\mathbf{v} d\Omega \tag{5}$$

was monitored. The evolution of the kinetic energy dissipation rate $\epsilon = -\frac{dE_k}{dt}$ was computed by differentiating the 8th order polynomial fit given by the temporal quadrature points and lifted with the jump across temporal element boundaries.

We assess the quality of our numerical solutions by computing individual terms in the kinetic energy evolution equation. For incompressible flow the kinetic energy dissipation rate is equal to $2\mu\mathcal{E}$, where $\mathcal{E}$ is the enstrophy, computed as:

$$\mathcal{E} = \frac{1}{\Omega}\int_\Omega \tfrac{1}{2}\rho \boldsymbol{\omega}\cdot\boldsymbol{\omega} d\Omega \tag{6}$$

where $\boldsymbol{\omega} = \nabla\times\mathbf{v}$ is the vorticity. For compressible flow, the kinetic energy dissipation rate is given by the sum of three contributions $\epsilon = \epsilon_1 + \epsilon_2 + \epsilon_3 = -\frac{dE_k}{dt}$:

$$\epsilon_1 = \frac{1}{\Omega}\int_\Omega 2\mu\,\mathbf{S}:\mathbf{S}\,d\Omega \tag{7}$$

$$\epsilon_2 = \frac{1}{\Omega}\int_\Omega \lambda\left(\nabla\cdot\mathbf{v}\right)^2 d\Omega \tag{8}$$

$$\epsilon_3 = -\frac{1}{\Omega}\int_\Omega p\,\nabla\cdot\mathbf{v}\,d\Omega \tag{9}$$

where $\mathbf{S} = \frac{1}{2}(\nabla\mathbf{v} + \nabla\mathbf{v}^T)$ is the strain rate tensor. We note that $\mathcal{E}$, ϵ_1, ϵ_2 and ϵ_3 are computed using the "lifted" gradients in order to be consistent with our DG discretization.

Since the flow is nearly incompressible, we expect that the dissipation due to the bulk viscosity (ϵ_2) and the pressure strain term (ϵ_3) to be small. The kinetic energy dissipation rate is then approximately equal to $\epsilon \approx 2\mu\mathcal{E} \approx \epsilon_1$. Differences between these quantities indicates the presence of compressibility effects and numerical dissipation.

Figure 1 plots the dimensionless viscous dissipation ϵ_1 vs time for 2nd-, 4th-, 8th, and 16-order schemes on all meshes considered. Figure 1 also plots the dissipation computed for an incompressible simulation using a spectral code on a 512^3 grid [7]. Even on the finest mesh considered the second-order scheme resolves barely more than half of the viscous dissipation. In contrast the 16th-order scheme resolves a significantly larger portion of the viscous dissipation on the coarses mesh considered.

Figure 2 shows the error in the kinetic energy dissipation rate for the cases considered. For the same number of degrees of freedom, increasing the polynomial order reduces the error. However, we are primarily interested in the computational cost to reach a particular error leve. In Figure 3 we present the error versus work units. Once again, the higher-order methods are more efficient than the low order scheme, in particular when a low error tolerance is required. We note that the 16th-order scheme has a lower error level on the coarsest mesh than the 2nd-order scheme on the finest mesh with a computational cost 3 orders of magnitude less. Finally we summarize the cases run in Table .

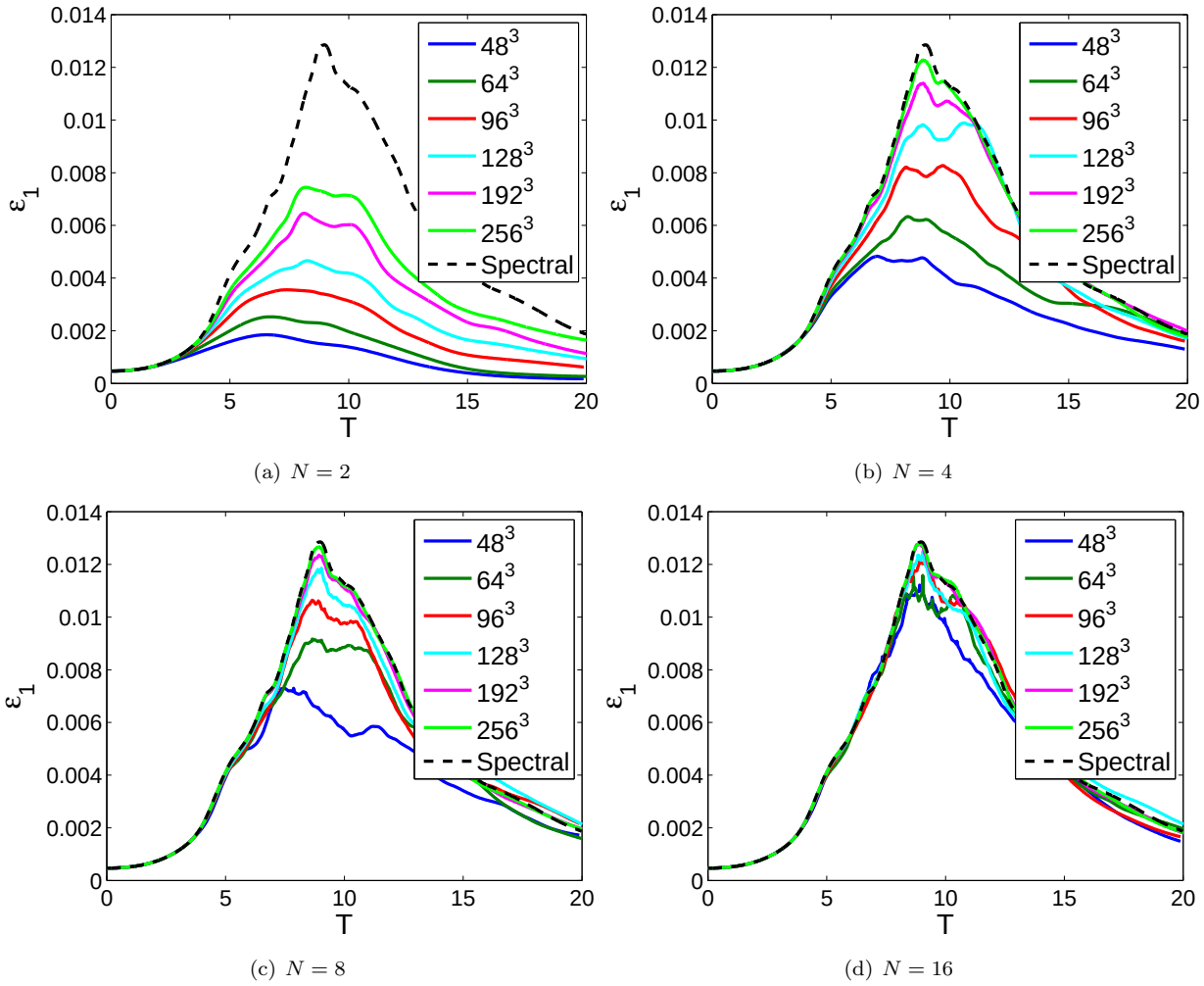

(a) $N = 2$

(b) $N = 4$

(c) $N = 8$

(d) $N = 16$

Figure 1: Viscous dissipation due to strain for the Taylor-Green vortex evolution, $M_0 = 0.1$, $Re = 1600$.

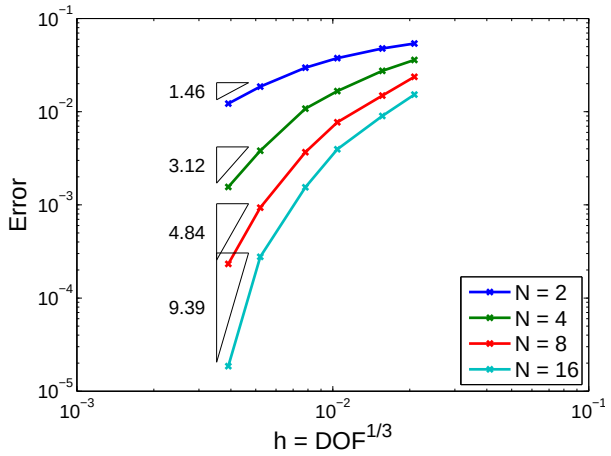

Figure 2: Kinetic energy dissipation rate error vs h for the Taylor-Green vortex evolution, $M_0 = 0.1$, $Re = 1600$.

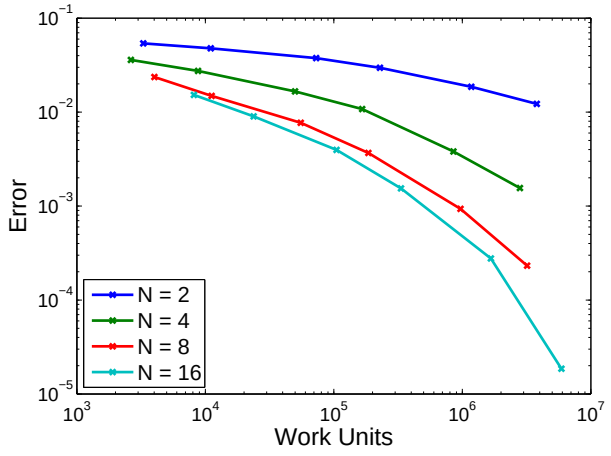

Figure 3: Kinetic energy dissipation rate error vs. work units for the Taylor-Green vortex evolution, $M_0 = 0.1$, $Re = 1600$.

N	1/h	Work Units	Error
2	48	3.29×10^3	5.40×10^{-2}
2	64	1.10×10^4	4.78×10^{-2}
2	96	7.28×10^4	3.76×10^{-2}
2	128	2.28×10^5	2.97×10^{-2}
2	192	1.17×10^6	1.86×10^{-2}
2	256	3.79×10^6	1.22×10^{-2}
4	48	2.64×10^3	3.60×10^{-2}
4	64	8.77×10^3	2.74×10^{-2}
4	96	4.99×10^4	1.66×10^{-2}
4	128	1.66×10^5	1.08×10^{-2}
4	192	8.52×10^5	3.81×10^{-3}
4	256	2.80×10^6	1.56×10^{-3}
8	48	4.02×10^3	2.37×10^{-2}
8	64	1.12×10^4	1.49×10^{-2}
8	96	5.53×10^4	7.70×10^{-3}
8	128	1.86×10^5	3.68×10^{-3}
8	192	9.68×10^5	9.35×10^{-4}
8	256	3.19×10^6	2.32×10^{-4}
16	48	8.15×10^3	1.53×10^{-2}
16	64	2.38×10^4	9.02×10^{-3}
16	96	1.05×10^5	3.96×10^{-3}
16	128	3.33×10^5	1.54×10^{-3}
16	192	1.67×10^6	2.76×10^{-4}
16	256	5.91×10^6	1.86×10^{-5}

Table 1: Taylor-Green Vortex case summaries

References

[1] Diosady, L. T. and Murman, S. M., "Design of a variational multiscale method for turbulent compressible flows," AIAA Paper 2013-2870, 2013.

[2] Diosady, L. T. and Murman, S. M., "DNS of flows over periodic hills using a discontinuous Galerkin spectral element method," AIAA Paper 2014-2784, 2014.

[3] Roe, P. L., "Approximate Riemann solvers, parameter vectors, and difference schemes," *Journal of Computational Physics*, Vol. 43, No. 2, 1981, pp. 357–372.

[4] Bassi, F. and Rebay, S., "GMRES discontinuous Galerkin solution of the compressible Navier-Stokes equations," *Discontinuous Galerkin Methods: Theory, Computation and Applications*, edited by K. Cockburn and Shu, Springer, Berlin, 2000, pp. 197–208.

[5] Diosady, L. T. and Murman, S. M., "Tensor-Product Preconditioners for Higher-order Space-Time Discontinuous Galerkin Methods," 2014, in preparation.

[6] Wang, Z., Fidkowski, K., Abgrall, R., Bassi, F., Caraeni, D., Cary, A., Deconinck, H., Hartmann, R., Hillewaert, K., Huynh, H., Kroll, N., May, G., Persson, P.-O., van Leer, B., and Visbal, M., "High-Order CFD Methods: Current Status and Perspective," *International Journal for Numerical Methods in Fluids*, Vol. 72, 2013, pp. 811–845.

[7] van Ress, W., Leonard, A., Pullin, D., and Koumoutsakos, P., "A comparison of vortex and pseudo-spectral methods for the simulation of periodic vortical flows at high Reynolds number," *Journal of Computational Physics*, Vol. 230, 2011, pp. 2794–2805.